catalysts

MDPI

Article

Ni Catalysts Supported on Modified Alumina for Diesel Steam Reforming

Antonios Tribalis [1], George D. Panagiotou [1], Kyriakos Bourikas [2], Labrini Sygellou [3,4], Stella Kennou [3], Spyridon Ladas [3], Alexis Lycourghiotis [1] and Christos Kordulis [1,4,*]

Received: 12 November 2015; Accepted: 7 January 2016; Published: 13 January 2016
Academic Editor: Michalis Konsolakis

1 Department of Chemistry, University of Patras, GR-26504 Patras, Greece; atribalis@hotmail.com (A.T.); geopangio@gmail.com (G.D.P.); alycour@upatras.gr (A.L.)
2 School of Science and Technology, Hellenic Open University, GR-26222 Patras, Greece; bourikas@eap.gr
3 Department of Chemical Engineering, University of Patras, GR-26504 Patras, Greece; sygellou@iceht.forth.gr (L.S.); kennou@chemeng.upatras.gr (S.K.); ladas@chemeng.upatras.gr (S.L.)
4 Institute of Chemical Engineering Science (FORTH/ICE-HT), Stadiou Str. Platani, P.O. Box 1414, GR-26500 Patras, Greece
* Correspondence: kordulis@upatras.gr; Tel.: +30-2610-969-883; Fax: +30-2610-996-041

Abstract: Nickel catalysts are the most popular for steam reforming, however, they have a number of drawbacks, such as high propensity toward coke formation and intolerance to sulfur. In an effort to improve their behavior, a series of Ni-catalysts supported on pure and La-, Ba-, (La+Ba)- and Ce-doped γ-alumina has been prepared. The doped supports and the catalysts have been extensively characterized. The catalysts performance was evaluated for steam reforming of *n*-hexadecane pure or doped with dibenzothiophene as surrogate for sulphur-free or commercial diesel, respectively. The undoped catalyst lost its activity after 1.5 h on stream. Doping of the support with La improved the initial catalyst activity. However, this catalyst was completely deactivated after 2 h on stream. Doping with Ba or La+Ba improved the stability of the catalysts. This improvement is attributed to the increase of the dispersion of the nickel phase, the decrease of the support acidity and the increase of Ni-phase reducibility. The best catalyst of the series doped with La+Ba proved to be sulphur tolerant and stable for more than 160 h on stream. Doping of the support with Ce also improved the catalytic performance of the corresponding catalyst, but more work is needed to explain this behavior.

Keywords: nickel catalyst; diesel steam reforming; doping; basicity; TPR; DRS; XPS; PEM-Fuel Cells

1. Introduction

PEM (proton-exchange membrane) fuel cell technology promises to be an efficient and clean alternative with respect to fuel combustion for primary power generation in stationary and mobile source applications. All fuel cells currently being developed for near term use in electric vehicles require hydrogen as a fuel. Hydrogen can be stored directly or produced onboard the vehicle by reforming methanol, or hydrocarbon fuels derived from crude oil—e.g., gasoline, diesel, or middle distillates. The vehicle design is simpler with direct hydrogen storage, but requires the development of a more complex refuelling infrastructure [1]. Thus the H_2 production onboard by the catalytic reforming of liquid fuels is very attractive [2]. Hence, there is great interest in converting hydrocarbons and oxygenated hydrocarbons into hydrogen. The process of converting petroleum fuels to hydrogen-rich gas products that have been developed in the past generally fall into one of the following classes—steam reforming (SR), partial oxidation (POX), autothermal reforming (ATR), dry reforming (DR) or a combination of two or more of the above. Despite their advantages, each of these processes has drawbacks with respect to design, fuel, and operating temperature [3]. The choice of reforming processes for producing

fuel-cell feeds of the necessary quality has been thermodynamically analyzed using different fuels [4]. Similarly, the challenges and opportunities of various fuel reforming technologies for application in low and high-temperature fuel cells have been thoroughly reviewed [5].

Fuels produced by pure steam-reforming contain ~70%–80% hydrogen [6] proving this process the most productive one. Recently, Remiro *et al.* [7] have reported on the possibility to obtain an almost pure H_2 stream (99% H_2) by in situ capturing of CO_2 produced in the steam reforming process. Fuels, such as natural gas, methanol, propane, gasoline, or aqueous bio-oil/bio-ethanol mixtures have been widely studied for their reforming characteristics [8–12]. Due to the complexity of diesel fuel, its conversion by steam reforming is a complicated problem [13].

The design of a fuel reforming catalyst is a difficult undertaking. Weight, size, activity, cost, transient operations, versatility to reform different fuels/compositions, catalyst durability, and fuel processor efficiency are critical considerations for both stationary and automotive fuel cell applications. A desirable catalyst is one which catalyzes the reaction at low temperatures and is resistant to coke formation and tolerant for various concentrations of poison (e.g. sulfur, halogens, heavy metals, *etc.*) for extended periods of time [2].

Generally, reforming catalysts consist of a base metal (Ni, Co, *etc.*) promoted by a noble metal (Pt, Pd, Rh, Ru, *etc.*) supported on stabilized supports (alumina, ceria, ceria promoted alumina, zeolite, *etc.*) [14]. Steam reforming Ni-based catalysts are the most popular. Although these catalysts are cost effective and commercially available, they have a number of drawbacks when considered for fuel cell applications. For instance, they have a high propensity toward coke formation, whereas in their active state they are pyrophoric and intolerant to sulfur. Diesel is a complex hydrocarbon mixture characterized by the presence of sulphur. Even though desulfurization can be used to remove most of the sulphur from a traditional fuel, the small quantities that remain (10 ppm in EU since 2010) can lead to deactivation after many hours on stream.

In the present work, we have tried to minimize the above mentioned drawbacks of the Ni-based steam reforming catalysts by preparing such catalysts supported on modified alumina. Alumina has been chosen, as it has several advantages in comparison with other ceramic materials: it is inexpensive, quite highly refractory, and supposedly relatively inert to water in the range of the SR process conditions [15]. BaO, La_2O_3, and CeO_2 have been used as modifiers, as these materials have already been tried in similar processes, namely catalytic partial oxidation of hydrocarbons [16]. Although La and Ce-promoted Ni/γ-Al_2O_3 catalysts have been reported in the steam reforming of light hydrocarbons [17–19], there are few studies on the rare-earth promoted catalysts in the diesel steam reforming [20]. The prepared catalysts have been characterized by using a combination of N_2 adsorption-desorption, X-ray diffraction (XRD), UV-Vis diffuse reflectance spectroscopy (DRS), temperature programmed reduction (TPR), X-ray photoelectron spectroscopy (XPS), and microelectrophoresis techniques.

The catalysts' performance was evaluated in a fixed bed micro-reactor using *n*-hexadecane with or without dibenzothiophene doping as surrogate for desulphurized commercial (10 ppm S) or sulphur free diesel, respectively. Thus, we attempted to gain insight concerning the influence of support modification on carbon deposition and sulfur poisoning during steam reforming.

2. Results and Discussion

2.1. Physicochemical Characteristics of the Supports

Five supports, pure alumina as well as La-, Ba-, (La+Ba)-, Ce-doped alumina, were used for the preparation of nickel catalysts studied in the present work. The doped supports were prepared by wet impregnation of pure alumina with aqueous solutions of the nitrate salts of the above ions. The composition, specific surface areas, and isoelectric points of these supports are shown in Table 1.

Table 1. Dopant content, specific surface areas calculated per gram of support (SSA_S) and per gram of alumina (SSA_{Al}), and isoelectric points (IEP) of the supports used.

Supports	Dopant Content (% mole)			SSA_S (m^2/g)	SSA_{Al} (m^2/g of Al_2O_3)	IEP
	La	Ba	Ce			
Al	-	-	-	152	152	7.98
Al-La	3	-	-	145	159	8.91
Al-Ba	-	10	-	128	149	8.98
Al-(La+Ba)	3	10	-	117	150	9.70
Al-Ce	-	-	3	162	170	7.88

Inspection of this table shows that the doping of alumina by La, Ba or (La+Ba) results in doped supports with specific surface areas (S_{BET}) lower than that of the parent alumina. However, the calculation of the surface area per gram of alumina ($S_{BET/Al}$) results in values equal to that of undoped alumina. This indicates no pore blockage of the support and eventually quite good dispersion of the dopant on the support surface. In contrast, doping with Ce provoked a slight increase in the specific surface area due to the porous nature of the corresponding oxide itself.

Figure 1 presents the pore size distributions of the prepared supports. One can observe a very small narrowing of the distributions along with a small shift towards lower pore diameters. This picture corroborates that no pore blockage takes place upon doping.

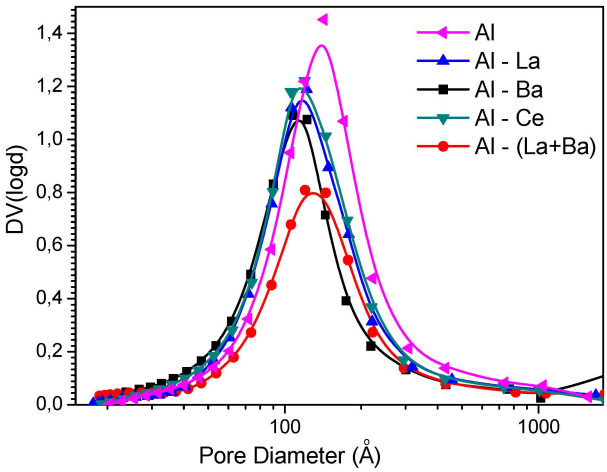

Figure 1. Pore size distributions of the supports used.

Figure 2 illustrates the XRD patterns of the supports used for the preparation of the corresponding Ni-catalysts. These patterns have been recorded after calcination at 850 °C. Diffraction peaks at 2θ = 37.2, 45.8, and 66.7° correspond to γ-Al_2O_3 (JCPDS 86-1410). The most intensive of these three peaks are visible in the patterns of all the supports studied.

Diffraction peaks assigned to crystalline species of either La_2O_3 (JCPDS 83-1355) or $LaAlO_3$ (JCPDS 85-1071) were not observed in the Al-La support. However, the corresponding pattern shows that doping with La decreases the alumina crystallinity broadening the corresponding peaks. Doping with Ba provoked a similar effect on the alumina crystallinity, while additional diffraction peaks, with the most intensive at 2θ = 28.3°, indicate the formation of $BaAl_2O_4$ phase (JCPDS 82–2001). The formation of the latter is much more pronounced in the support doped with La+Ba. Doping with Ce had a little influence on the alumina crystallinity, while a diffraction peak arising at 2θ = 28.6° suggests the segregation of a CeO_2-phase (JCPDS 081-0792) over the γ-Al_2O_3 surface [21]. The formation of a porous CeO_2 phase explains the increase of the specific surface area of the Al-Ce support discussed previously (see Table 1).

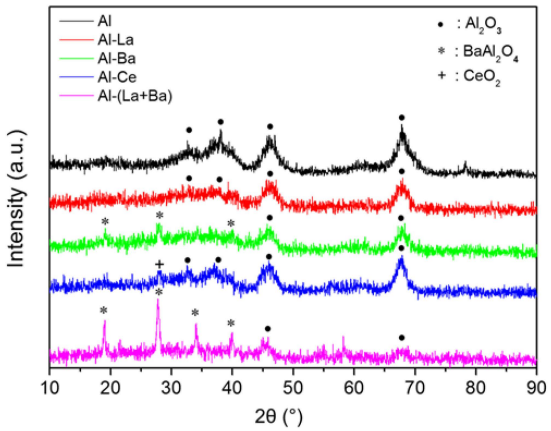

Figure 2. XRD patterns of pure (Al) and doped with La (Al-La), Ba (Al-Ba), Ce (Al-Ce), and La+Ba (Al-(La+Ba)) alumina after calcination at 850 °C.

The isoelectric point (IEP) values in Table 1 show that the doping with La and/or Ba increases the basicity of alumina, while the doping with Ce has a slightly opposite action. It is well known that the acid-base properties of the support influence the deposition mechanism of the active phase [22] and, thus, the active species formed on the support surface, as well as the resistance of the final catalyst to coke formation. It has been shown that the rate of carbon deposition on catalyst surfaces is reduced when the active metal is supported on a more basic carrier [23,24].

2.2. Physicochemical Characteristics of the Ni-Catalysts

The Ni-catalysts studied were prepared by wet impregnation of the support with a $Ni(NO_3)_2$ aqueous solution of appropriate concentration to obtain catalysts with Ni loading equal to 15wt. %. Comparing the specific surface areas of the final Ni-catalysts (SSA_C) presented in Table 2 with those of the corresponding supports (SSA_S) compiled in Table 1, we observe that the deposition of Ni caused a decrease of the specific surface area of ~20% in the case of the doped samples. This decrease was smaller in the undoped catalyst (~13%), which might indicate a higher dispersion of the Ni-phase in the undoped catalyst or a relatively high extent of $NiAl_2O_4$ formation by incorporation of Ni^{2+} ions into the alumina lattice.

Figure 3 shows the pore size distributions of the prepared catalysts. Similar distributions can be observed for all catalysts. However, in the Ni/Al sample a slightly higher contribution of small pores can be observed, in agreement with our previous comments for the Ni deposited on the surface of un-doped alumina.

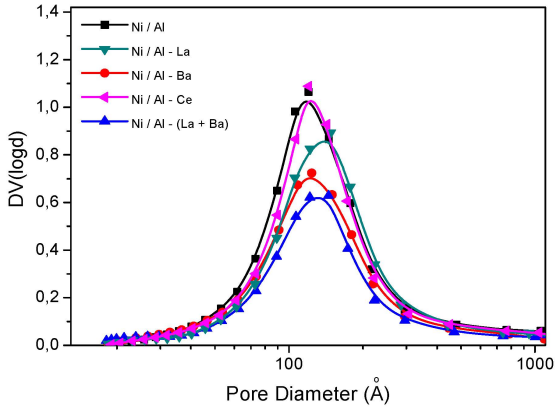

Figure 3. Pore size distributions of the catalysts studied.

Table 2. Specific surface areas of the catalysts (SSA_C), their crystal phases detected by XRD, their $NiAl_2O_4$/NiO ratios determined by DRS (R_{DRS}) and TPR (R_{TPR}) and percentage of Ni reduced upon TPR measurements (% Ni^0).

Catalysts	SSA_C (m^2/g)	Crystal Phases Detected by XRD	R_{DRS}	R_{TPR}	% Ni^0
Ni/Al	132	$NiAl_2O_4$, γ-Al_2O_3	4.86	3.75	79.9
Ni/Al-La	112	$NiAl_2O_4$, γ-Al_2O_3	4.67	1.94	87.4
Ni/Al-Ba	105	$BaAl_2O_4$, $NiAl_2O_4$, γ-Al_2O_3	3.11	1.67	86.1
Ni/Al-(La+Ba)	91	$BaAl_2O_4$, $NiAl_2O_4$, γ-Al_2O_3	2.63	1.50	98.1
Ni/Al-Ce	124	CeO_2, $NiAl_2O_4$, γ-Al_2O_3	4.82	3.80	77.3

Figure 4 shows the XRD patterns of the Ni-catalysts studied after calcination at 850 °C. The diffraction peaks observed in the XRD patterns of the corresponding supports (see Figure 2) can be also found in these patterns. A careful inspection of Figure 4 reveals that there is no evidence of a NiO phase (37.3, 43.3, and 62.9 JCPDS 78-0643). On the other hand, diffraction peaks attributed to $NiAl_2O_4$ crystallites can be found in the XRD patterns of all catalysts studied. Although, it is difficult to discriminate between $NiAl_2O_4$ and γ-Al_2O_3 from their XRD patterns, because almost all the diffraction peaks of these phases overlap, they can be distinguished from each other by the peak intensities of the main diffractions. Table 2 summarizes the crystal phases detected in the calcined Ni-catalysts.

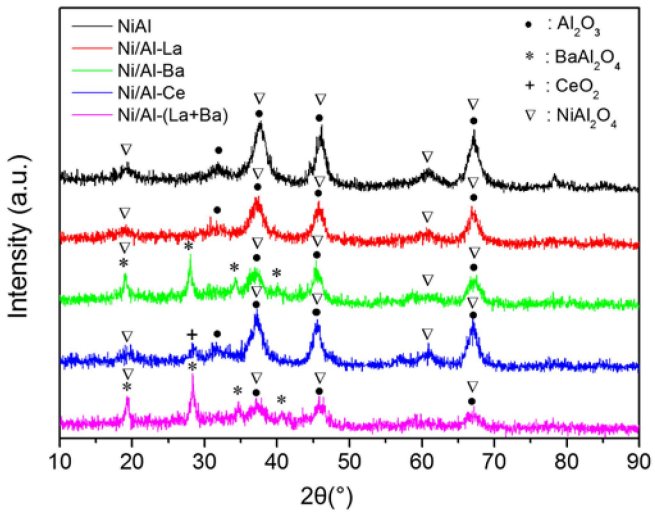

Figure 4. XRD patterns of Ni-catalysts supported on pure (Ni/Al) and doped with La (Ni/Al-La), Ba (Ni/Al-Ba), Ce (Ni/Al-Ce), and La+Ba (Ni/Al-(La+Ba)) alumina after calcination at 850 °C.

The formation of $NiAl_2O_4$ crystallites is attributed to the fact that Ni^{2+} ions preferentially incorporate into the tetrahedral vacancies of γ-Al_2O_3 at low nickel loading [25]. However, detailed analysis of the XRD patterns revealed that the $NiAl_2O_4$ content of the catalysts prepared depends on the alumina doping. More precisely, $NiAl_2O_4$ seems to be the predominant nickel phase in the Ni/Al sample. Its content decreases in the catalyst prepared using La doped alumina. La-phase has not been detected in the latter sample confirming its very good dispersion suggested by the SSA results discussed previously (Table 1).

Doping of alumina with Ba caused, in addition, the formation of $BaAl_2O_4$ as new peaks appeared in the corresponding XRD pattern at 2θ: 19.08°, 27.85°, 34.24°, and 40.09° [26]. The formation of this crystal phase seems to take place by insertion of Ba^{2+} ions into γ-Al_2O_3 lattice maintaining intact the corresponding SSA_{Al} (see Table 1). In such a case the Ba^{2+} insertion probably competes with the insertion of the Ni^{2+} ions for the same alumina lattice vacancies. This is corroborated by the observation that the intensities of the peaks assigned to $NiAl_2O_4$ are lower in the XRD pattern of Ni/Al-Ba sample

than those recorded in the previous samples. Thus, the doping of alumina with Ba leads to a decrease of $NiAl_2O_4$ content in the corresponding catalyst. The XRD pattern of Ni/Al-(La+Ba) catalyst was similar to that of Ni/Al-Ba one. However, the $NiAl_2O_4$ content of the doubly doped catalyst seems to be the lowest detected among the catalysts studied in the present work. The XRD pattern of Ni/Al-Ce catalyst showed the formation of CeO_2 crystallites in addition to those of γ-Al_2O_3 and $NiAl_2O_4$.

Figure 5 illustrates the diffuse reflectance (DR) spectra of the prepared catalysts recorded in the range 500–800 nm. An intense doublet with maxima at 595 and 635 nm appears in these spectra. This doublet is assigned to Ni^{2+} ions in tetrahedral symmetry and thus it is associated with the formation of the $NiAl_2O_4$ phase detected by XRD. Two shoulders appearing at 561 and 715 nm are assigned to Ni^{2+} ions in octahedral symmetry associated with the NiO phase [27,28].

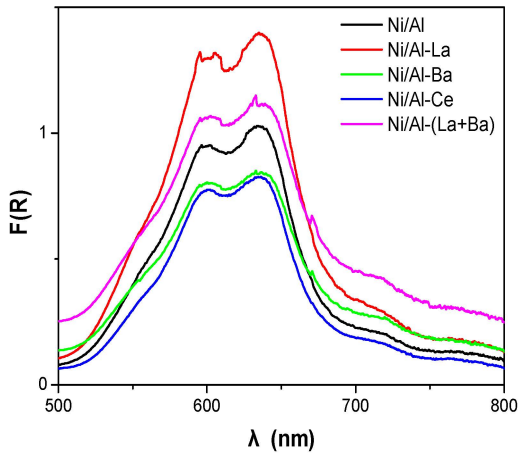

Figure 5. Diffuse reflectance spectra of the catalysts recorded in the range 500–800 nm.

To study the effect of doping on the catalysts, it is necessary to analyze the peaks of various Ni^{2+} species. However, the quantitative analysis of these species based on the DR spectra is relatively difficult because of the overlapping of the absorption domains of various Ni^{2+} ions. Thus, for obtaining a rough indication of the relative content of $NiAl_2O_4$ to NiO we used the ratio (R_{DRS}) of the height of the peak at 635 nm to the height of the peak at 715 nm [29].

The R_{DRS} values for the catalysts studied are included in Table 2. Taking into account these values one can conclude that doping of alumina with La and Ba decreases the $NiAl_2O_4$ content of the catalysts in accordance with XRD results mentioned before. More precisely, the $NiAl_2O_4$ content of the catalysts follows the order Ni/Al > Ni/Al-La > Ni/Al-Ba > Ni/Al-(La+Ba). On the other hand, doping of alumina with Ce does not influence the relative amount of $NiAl_2O_4$/NiO.

The reducibility of the Ni-species and their interaction with the support were studied via TPR experiments. It is evident from the TPR profiles (Figure 6) that the catalysts consume hydrogen in three temperature ranges. The first and minor peak appears at 350 °C but only in the TPR profile of Ni/Al-Ce catalyst. It is assigned to the reduction of loosely attached NiO crystals. The small size of this peak shows that the relative amount of these crystals is very low. According to the literature [30,31], doping of Ni-catalysts with Ce promotes the NiO reduction due to action of the Ce^{3+}/Ce^{4+} redox pairs, which facilitate electron transfer.

The second and relatively more intense event characterized by a broad peak appearing in all TPR profiles, with maxima in the range 400–650 °C, arises from the reduction of NiO species exhibiting stronger interaction with the support. The fact that the peak is broad and asymmetric indicates the presence of a multitude of such NiO species with different strength of binding to the support [32,33]. The third and most important reduction event appears at 817 ± 10 °C. The corresponding well resolved peak should be assigned to the reduction of the $NiAl_2O_4$ phase [34] detected by XRD and DRS.

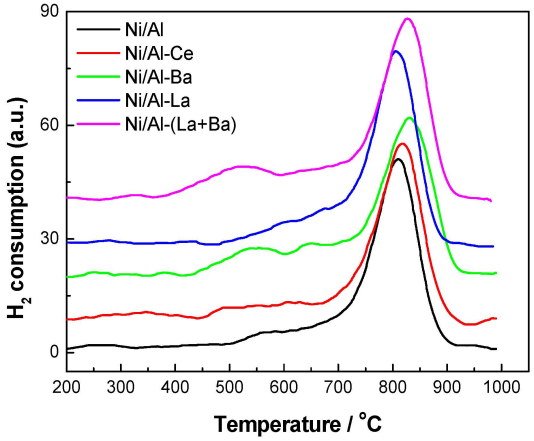

Figure 6. TPR profiles of the prepared catalysts recorded in the temperature range 150–1000 °C.

Deconvolution of the TPR curves has been performed in order to calculate the $NiAl_2O_4$/NiO ratio (R_{TPR}). The corresponding values are given in Table 2. These values follow the same trend as those calculated from the DR spectra.

Taking into account the amount of hydrogen required for complete reduction of the supported Ni ($Ni^{2+} \rightarrow Ni^0$) and the total amount of hydrogen experimentally consumed, the percentage of Ni-phase reduced upon TPR measurements (experimental/theoretical amount of hydrogen consumed) is obtained. The percentage values of this parameter (%Ni^0) are illustrated in the last column of Table 2. An inspection of these values reveals that doping with La and Ba and especially the combined doping with La and Ba increases the reducibility of the Ni-phase. These results are in good agreement with the decrease of the $NiAl_2O_4$ content in the corresponding catalysts indicated by the XRD and DRS results. In contrast, doping with Ce seems to have a slight, if any, negative effect on the total reducibility of Ni-phase, although, as already mentioned, it facilitated the reduction of NiO loosely bound on the support surface. Taking into account the corresponding R value appearing in Table 2, which indicates relatively higher $NiAl_2O_4$ content in the Ni/Al-Ce catalyst, this behavior could be easily explained.

The surface analysis of the catalysts prepared was performed by X-ray photoelectron spectroscopy (XPS). XPS resulted in the expected detection of Ni, Al, and O on the surfaces of all catalysts studied, as well as of La in Ni/Al-La and Ni/Al-(La+Ba) catalysts, Ba in Ni/Al-Ba and Ni/Al-(La+Ba) catalyst and Ce in the Ni/Al-Ce one. Organic carbon from a surface contamination layer, which consists mainly of CH_x with the dominant C1s peak set at 284.8 eV as a binding energy (BE) reference and some organic oxygen of the CO_x type, was found in all specimens due to the atmospheric exposure. The quantitative surface analysis of the catalysts was based on the following peaks: $Ni2p_{3/2}$ (855.9 eV), O1s (531.0 eV), Al2s (118.9 eV), $Ba3d_{5/2}$ (780.2 eV), $La3d_{5/2}$ (835.2 eV), and $Ce3d_{5/2}$ (~885 eV).

Table 3 summarizes the results obtained from the quantitative analysis of the XPS data, based on measured peak areas, one for each detected element as mentioned above, and taking into account the respective relative sensitivity factors (RSF).

Table 3. Quantitative surface analysis of the prepared catalysts based on XPS results.

Catalysts	Average Surface Composition (atoms %)					
	Ni	Al	O	La	Ba	Ce
Ni/Al	2.5	32.5	65.0	-	-	-
Ni/Al-La	2.8	28.2	67.9	1.1	-	-
Ni/Al-Ba	5.1	28.6	64.7	-	1.6	-
Ni/Al-(La+Ba)	5.4	24.4	67.3	1.4	1.5	-
Ni/Al-Ce	2.6	32.3	64.9	-	-	0.2

Inspection of Table 3 reveals that doping of the γ-Al_2O_3 carrier with La leads to only a slight surface enrichment of the corresponding catalyst with Ni-species. This effect becomes more intense by doping with Ba and even more intense when combined doping with La and Ba takes place. This surface enrichment with Ni-species is in good accordance with the increase of reducibility of these catalysts and the decrease in the R value discussed previously.

Although we do not have direct experimental measurement for Ni particle size (e.g., TEM), the XPS data (Table 3) offer strong evidence of enhanced Ni dispersion over the Ba-doped support. The measured Ni/Al atomic ratio on the Ba-doped alumina is more than two times larger than in the case of undoped alumina, whereas Ba has a tendency to be incorporated in alumina and not to cover it. Indeed the surface atomic concentration of Ba in the Ni/Al-Ba and Ni/Al-(La+Ba) catalysts was found to be relatively low compared to the nominal Ba concentration. This suggests the easy insertion of Ba ions into the alumina lattice and is in very good agreement with our XRD results, which indicated the formation of $BaAl_2O_4$ crystals (see Table 2). Doping with Ce seems to have a slight, if any, positive influence on the surface enrichment of Ni-species, while the surface concentration of Ce atoms was found to be extremely low. The latter effect can be explained by the formation of relatively large CeO_2 crystallites, as suggested also by XRD.

2.3. Catalyst Evaluation

The catalytic performance of the catalysts studied was evaluated in a fixed bed micro-reactor for the steam reforming of hexadecane (surrogate sulphur-free diesel) and hexadecane doped with dibenzothiophene corresponding to surrogate commercial diesel with 10 ppm sulphur. The only products detected in the gas stream at the reactor outlet were H_2, CO, CO_2 and CH_4. Figure 7 shows the production rate of H_2 measured over the Ni-catalysts supported on pure, La-, Ba-, and (La+Ba)-doped γ-Al_2O_3. Complete conversion of *n*-hexadecane was observed at 795 °C over all of the catalysts studied in accordance with the results described recently by Kaynar *et al.* [35].

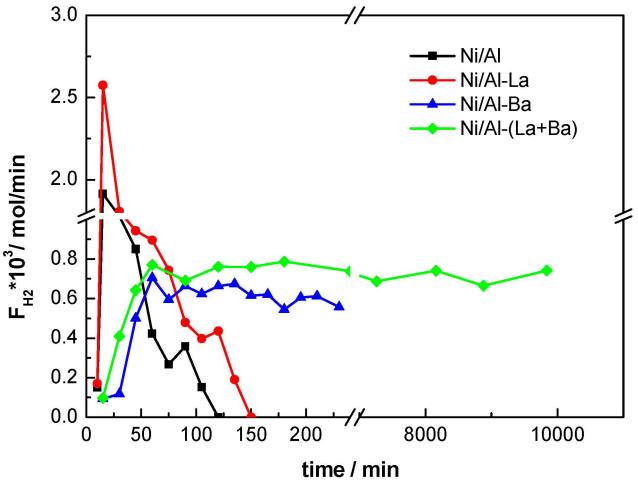

Figure 7. Hydrogen production rates measured over the Ni-catalysts supported on pure (■), La- (●), Ba- (▲), and (La+Ba)- (◆) modified γ-Al_2O_3 with the time on stream. (Reaction conditions: Steam to Carbon ratio = 2.67, Reaction temperature: 795 °C, catalyst mass = 0.05 g, GHSV= 20000 h^{-1})

In all catalytic runs the H_2 mass flow rates (F) measured at the reactor outlet increased initially and reached their maximum value after 0.5–1 h on stream. This is in accordance with the fact that metallic nickel is the active phase of the catalysts studied, while the reactor was loaded with their oxide form. Thus, the initial increase of H_2 production rate should be attributed to the in situ activation (reduction) of the catalyst by the H_2 produced (see Experimental section). The Ni/Al and Ni/Al-La catalysts exhibited important initial activities (after ~0.5 h on stream) but they were fully deactivated

after 2 and 2.5 h on stream, respectively. However, the beneficial action of doping with La was clear resulting in higher initial activity and longer deactivation time compared to that of un-doped catalyst. The enhanced initial H_2 production observed over the Ni/Al and Ni/Al-La samples can be attributed to decomposition of the hydrocarbon, which is expected to increase the coke formation over the catalysts, thus explaining the simultaneous rapid deactivation of these samples [35]. Coke formation in the form of both amorphous and graphitic filamentous carbon was identified as the main reason for deactivation of rich in $NiAl_2O_4$ catalysts studied by Jiménez-González *et al.* [11] for steam reforming of isooctane.

Doping of the catalyst support with Ba or (Ba+La) further improved the catalytic performance of the corresponding samples (Figure 7). This improvement could be attributed to the following effects caused by doping with Ba or (Ba+La): surface enrichment of the nickel phase as observed by the XPS analysis, decrease of the support acidity measured by microelectrophoresis and increase of the Ni-phase reducibility determined by TPR. Taking into account that all the catalysts studied in the present work had the same Ni loading, their surface enrichment with nickel phase caused by doping of the support with Ba or Ba+La indicates an increase of the dispersion of the active phase. Christensen *et al.* [36] reported that lower coking rates are possible for Ni-catalysts with higher metallic dispersion, and Quitete *et al.* [37] found that coke formation is favored by increasing nickel particle size. On the other hand, it is well known that low tendency to coke formation is observed when the Ni active phase is dispersed on less acidic supports [38]. As to the influence of Ni-phase reducibility on catalytic performance it is well known that metallic Ni atoms are active sites for the steam reforming of hydrocarbons [39].

Figure 8 shows the production rates of H_2, CO, CO_2, and CH_4 measured at the outlet of the reactor on a dry basis after 4 h on stream over all catalysts under sulfur free conditions and over the Ni/Al-(La+Ba) catalyst, which is the most promising one, in the presence of sulphur in the feed. Comparing the Ni/Al-Ba and Ni/Al-(La+Ba) catalysts one can observe that the enhanced H_2 production rate observed in the latter is accompanied by lower CH_4 and higher CO and CO_2 production rates. This probably shows that doping hinders the methanation reactions.

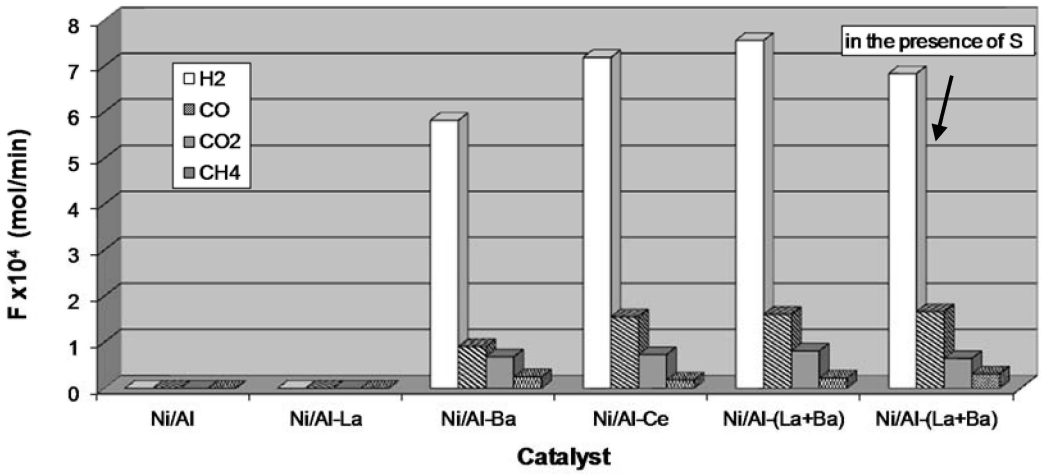

Figure 8. Production rates of H_2, CO, CO_2, and CH_4 after 4 h on stream over the catalysts under sulphur free conditions and over the Ni/Al-(La+Ba) catalyst in the presence of 10 ppm sulphur in the feed (Steam/Carbon ratio: 2.67, Reaction temperature: 795 °C, catalyst mass: 0.05 g, GHSV= 20000 h^{-1}).

The Ni/Al-(La+Ba) catalyst proved to be quite active even in the presence of sulphur in the stream because only a small decrease (<10%) in its activity has been observed when the reactor was fed with surrogate diesel containing 10 ppm sulphur. The activity of this most promising Ni/Al-(La+Ba) catalyst was tested for long times under sulphur free conditions and proved to be quite stable for more than 168 h on stream (see Figure 7).

Doping of the support with Ce caused also significant increase in the activity of the corresponding catalyst, which could not be explained taking into account the physicochemical characteristics of the Ni-phase examined in the present work. According to the literature, the beneficial action of Ce could be attributed to the scavenging of the coke from the surface of the Ni phase via oxygen provided by the CeO_x phase [40]. Indeed, this phase has been detected in our Ni/Al-Ce sample by XRD. However, more work is necessary in order to explain the important catalytic behavior of the Ni/Al-Ce sample.

3. Experimental Section

Alumina extrudates (AKZO, HDS-000-1,5mmE, SSA = 264 m^2/g, pore volume: 0.65 cm^3/g) were crushed and sieved to obtain a support powder with particle size 90–105 μm. It was wet impregnated with aqueous nitrate solutions of $La(NO_3)_3 \cdot 6H_2O$ (Sigma-Aldrich, Taufkirchen, Germany, 99.999%), $Ce(NO_3)_3 \cdot 6H_2O$ (Alfa Aesar, Lancashire, United Kingdom, 99.5%), and $Ba(NO_3)_2$ (Sigma-Aldrich, 99.999%) of volume equal to 20 times the total pore volume of the support used. The solution contained the appropriate amount of salt to obtain the desired concentration of dopant in the doped support and the final catalyst. After the evaporation of water in a rotary evaporator (BUCHI, Flawil, Switzerland) impregnates were dried overnight at 120 °C in air, then they were calcined by increasing the temperature initially up to 400 °C (3 °C/min) and then up to 850 °C (10 °C/min), where they remained for 3 h. A series of Ni catalysts supported on pure and modified alumina containing 15% *w*/*w* Ni, was prepared following the above described procedure for the deposition of the nickel phase using aqueous solution of $Ni(NO_3)_2$ $6H_2O$ (Sigma-Aldrich, Taufkirchen, Germany 98%). The final impregnates were submitted to the same thermal treatment (drying and calcination) with that described above for the preparation of the supports.

The determination of the specific surface area (S_{BET}) of the samples was based on the nitrogen adsorption–desorption isotherms recorded using a Micromeritics apparatus (Tristar 3000 porosimeter, Micromeritics, Aachen, Germany) and the corresponding software. Pore size distributions have been determined using the BJH method and the N_2 desorption curve.

XRD measurements were carried out with a D8 Advance X-Ray diffractometer, Bruker, Leiderdorp, The Netherlands, equipped with nickel-filtered Cu Ka (0.15418 nm) radiation source. The step size and the time per step were respectively fixed at 0.02° and 0.5 s in the range of $20^\circ \leqslant 2\theta \leqslant 80^\circ$.

The diffuse reflectance spectra of the calcined samples were recorded in the range 200–800 nm at room temperature. A UV-Vis spectrophotometer (Varian Cary 3, Agilent Technologies, Santa Clara, CA, USA) equipped with an integration sphere was used. The corresponding support was used as reference. The samples were mounted in a quartz cell. This provided a sample thickness greater than 3 mm to guarantee the "infinite" sample thickness.

The isoelectric points of the pure and modified alumina supports were determined using a Zetasizer Nano-ZS apparatus (Malvern, United Kingdom) equipped with a DTS 1060C-Clear disposable zeta cell (Malvern, United Kingdom).

XPS measurements were carried out on catalyst powders prepared as described above and pressed in a hollow aluminum metal receptacle. The experiments took place in a MAX200 (LEYBOLD/SPECS, Berlin, Germany) Electron Spectrometer using non-monochromatic MgK_α radiation (1253.6 eV) and an EA200-MCD analyzer (SPECS, Berlin, Germany) operated at a constant pass energy (PE) of 140 eV in order to maximize signal intensity while maintaining a resolution of the order of 1.1 eV. The analysis was performed along the surface normal and the analyzed specimen area was a ~4 × 7 mm^2 rectangle near the specimen center with a depth of analysis of the order of 10nm. The binding energy (BE) scale was corrected for electrostatic charging via the main C1s peak from surface contamination set at 284.8 eV BE, the uncertainty in the corrected values being of the order of ±0.15 eV. The relative sensitivity factor (RSF) database used for quantitative analysis has been adapted to the MAX200 spectrometer (SPECS, Berlin, Germany) operating conditions from the empirical collection of Wagner *et al.* [41], whereas the assignment of the BE for the various chemical states of the elements was made using an appropriate database [42].

The TPR experiments were performed in a laboratory-constructed equipment described elsewhere [43]. An amount of sample, 0.1 g, was placed in a quartz reactor and the reducing gas mixture (H_2/Ar: 5/95 v/v) was passed through it for 2 h with a flow rate of 40 mL min^{-1} at room temperature. Then the temperature was increased to 1000 °C with a constant rate of 10 °C min^{-1}. Reduction leads to a decrease of the hydrogen concentration of the gas mixture, which was detected by a thermal conductivity detector (TCD) (Shimadzu, Duisburg, Germany). The reducing gas mixture was dried in a cold trap (−95 °C) before reaching the TCD.

Catalytic performance of the prepared samples was evaluated using a stainless steel fixed-bed reactor (diameter: 1/4 inch) loaded with 0.05 g of catalyst in its oxide form diluted with 0.05 g of quartz sand. Helium from a cylinder was fed through mass flow-meter (Brooks) into a saturator containing hexadecane or hexadecane/dibenzothiophen to simulate sulfur-free diesel and a diesel containing 10ppm of sulfur, respectively. The temperature of the saturator was set at 153 °C for obtaining constant partial pressure of surrogate diesel in the He stream. Triply distilled water was fed to the latter stream with a syringe pump (Braintree Scientific Inc., Braintree, MA, USA). A steam/carbon ratio of 2.67 was ensured. The line from the saturator to the reactor entrance was maintained at 350 °C in order to avoid any condensation. Thus, a GHSV= 20000 h^{-1} was obtained. The reactor temperature was set at 795 ± 1 °C. The outlet stream of the reactor was analyzed after cooling and gas-liquid separation (at 0−5 °C). Two gas chromatographs (GC-8A and GC-14B, Shimadzu, Duisburg, Germany) equipped with thermal conductivity detectors and SUPELCO columns (100/120 Carbosieve SII 10ft × 1/8IN SS and 60/80 Carboxen 1000 15ft × 1/8IN SS) were used for the dry-base analysis of the gas products. Sampling was performed using six port valves every 15 minutes for the first four hours of each catalytic test and then every four hours for the long term test performed over the Ni/Al-(La+Ba) catalyst. A delay was observed in the evolution of H_2 in the outlet of the reactor. Thus the maximum H_2 production was observed after 0.5 h on stream over the Ni/Al and Ni/Al-La samples and after 1 h over the rest of the catalysts. The aforementioned delay of H_2 evolution is attributed to its consumption for the in situ activation (reduction) of the catalysts by the H_2 initially produced.

4. Conclusions

The main conclusions drawn from the present work can be summarized as follows:

Doping of the γ-alumina support with Ba or (La+Ba) resulted in Ni catalysts with improved activity and stability for surrogate diesel steam reforming. This improvement can be attributed to the increase of the dispersion of the nickel phase, the decrease of the support acidity and the increase of Ni-phase reducibility.

Doping of the support with Ce caused also significant increase in the activity of the corresponding catalyst.

The doubly doped (La+Ba) catalyst proved also to be sulphur tolerant and stable for more than 160 h on stream.

Author Contributions: A.T. performed the preparation, evaluation, N_2-physisorption, and XRD study of the catalysts. G.D.P. performed TPR experiments and data analysis. K.B. performed DRS and IEP measurements and data analysis. L.S., S.K., and S.L. performed XPS measurements and data analysis. A.L. and C.K. supervised the work and wrote the manuscript. All authors contributed to the revision of the manuscript.

Conflicts of Interest: The authors declare no conflict of interest.

References

1. Ogden, J.M.; Steinbugler, M.M.; Kreutz, T.G. A comparison of hydrogen, methanal and gasoline as fuels for fuel cell vehicles: implications for vehicle design and infrastructure development. *J. Power Sources* **1999**, *79*, 143–168. [CrossRef]
2. Farrauto, R.; Hwang, S.; Shore, L.; Ruettinger, W.; Lampert, J.; Giroux, T.; Liu, Y.; Ilinich, O. New material needs for hydrocarbon fuel processing: Generating hydrogen for the PEM fuel cell. *Annu. Rev. Mater. Res.* **2003**, *33*, 1–27. [CrossRef]

3. Cheekatamarla, P.K.; Finnerty, C.M. Reforming catalysts for hydrogen generation in fuel cell applications. *J. Power Sources* **2006**, *160*, 490–499. [CrossRef]
4. Semelsberger, T.A.; Brown, L.F.; Borup, R.L.; Inbody, M.A. Equilibrium products from autothermal processes for generating hydrogen-rich fuel-cell feeds. *Int. J. Hydrogen Energy* **2004**, *29*, 1047–1064. [CrossRef]
5. Song, C.S. Fuel processing for low-temperature and high-temperature fuel cells—Challenges, and opportunities for sustainable development in the 21st century. *Catal. Today* **2002**, *77*, 17–49. [CrossRef]
6. Brown, L.F. A comparative study of fuels for on-board hydrogen production for fuel-cell-powered automobiles. *Int. J. Hydrogen Energy* **2001**, *26*, 381–397. [CrossRef]
7. Remiro, A.; Valle, B.; Aramburu, B.; Aguayo, A.T.; Bilbao, J.; Gayubo, A.G. Steam reforming of the bio-oil aqueous fraction in a fluidized bed reactor with in situ CO_2 capture. *Ind. Eng. Chem. Res.* **2013**, *52*, 17087–17098. [CrossRef]
8. Zhang, Y.; Wang, W.; Wang, Z.Y.; Zhou, X.T.; Wang, Z.; Liu, C.-J. Steam reforming of methane over Ni/SiO_2 catalyst with enhanced coke resistance at low steam to methane ratio. *Catal. Today* **2015**, *256*, 130–136. [CrossRef]
9. Barrios, C.E.; Bosco, M.V.; Baltanas, M.A.; Bonivardi, A.L. Hydrogen production by methanol steam reforming: Catalytic performance of supported-Pd on zinc-cerium oxides' nanocomposites. *Appl. Catal. B* **2015**, *179*, 262–275. [CrossRef]
10. Hou, T.F.; Yu, B.; Zhang, S.Y.; Zhang, J.H.; Wang, D.Z.; Xu, T.K.; Cui, L.; Cai, W.J. Hydrogen production from propane steam reforming over $Ir/Ce_{0.75}Zr_{0.25}O_2$ catalyst. *Appl. Catal. B* **2015**, *168*, 524–530. [CrossRef]
11. Jimenez-Gonzalez, C.; Boukha, Z.; de Rivas, B.; Ramon Gonzalez-Velasco, J.; Ignacio Gutierrez-Ortiz, J.; Lopez-Fonseca, R. Behaviour of nickel-alumina spinel ($NiAl_2O_4$) catalysts for isooctane steam reforming. *Int. J. Hydrogen Energy* **2015**, *40*, 5281–5288. [CrossRef]
12. Remiro, A.; Valle, B.; Oar-Arteta, L.; Aguayo, A.T.; Bilbao, J.; Gayubo, A.G. Hydrogen production by steam reforming of bio-oil/bio-ethanol mixtures in a continuous thermal-catalytic process. *Int. J. Hydrogen Energy* **2014**, *39*, 6889–6898. [CrossRef]
13. Thormann, J.; Pfeifer, P.; Schubert, K.; Kunz, U. Reforming of diesel fuel in a micro reactor for APU systems. *Chem. Eng. J.* **2008**, *135*, S74–S81. [CrossRef]
14. Lakhapatri, S.L.; Abraham, M.A. Deactivation due to sulfur poisoning and carbon deposition on $Rh-Ni/Al_2O_3$ catalyst during steam reforming of sulfur-doped n-hexadecane. *Appl. Catal. A* **2009**, *364*, 113–121. [CrossRef]
15. Faure, R.; Rossignol, F.; Chartier, T.; Bonhomme, C.; Maître, A.; Etchegoyen, G.; del Gallo, P.; Gary, D. Alumina foam catalyst supports for industrial steam reforming processes. *J. Eur. Ceram. Soc.* **2011**, *31*, 303–312. [CrossRef]
16. Haynes, D.J.; Campos, A.; Smith, M.W.; Berry, D.A.; Shekhawat, D.; Spive, J.J. Reducing the deactivation of Ni-metal during the catalytic partial oxidation of a surrogate diesel fuel mixture. *Catal. Today* **2010**, *154*, 210–216. [CrossRef]
17. Sanchez-Sanchez, M.C.; Navarro, R.M.; Fierro, J.L.G. Ethanol steam reforming over $Ni/La-Al_2O_3$ catalysts: Influence of lanthanum loading. *Catal. Today* **2007**, *129*, 336–345. [CrossRef]
18. Sanchez-Sanchez, M.C.; Navarro, R.M.; Fierro, J.L.G. Ethanol steam reforming over $Ni/M_xO_y-Al_2O_3$ (M = Ce, La, Zr and Mg) catalysts: Influence of support on the hydrogen production. *Int. J. Hydrogen Energy* **2007**, *32*, 1462–1471. [CrossRef]
19. Lucredio, A.F.; Filho, G.T.; Assaf, E.M. Co/Mg/Al hydrotalcite-type precursor, promoted with La and Ce, studied by XPS and applied to methane steam reforming reactions. *Appl. Surf. Sci.* **2009**, *255*, 5851–5856. [CrossRef]
20. Xu, L.; Mi, W.; Su, Q. Hydrogen production through diesel steam reforming over rare-erth promoted $Ni/\gamma-Al_2O_3$ catalysts. *J. Nat. Gas Chem.* **2011**, *20*, 287–293. [CrossRef]
21. Campos, C.H.; Osorio-Vargas, P.; Flores-Gonzalez, N.; Fierro, J.L.G.; Reyes, P. Effect of Ni Loading on Lanthanide (La and Ce) Promoted $\gamma-Al_2O_3$ Catalysts Applied to Ethanol Steam Reforming. *Catal. Lett.* **2015**. [CrossRef]
22. Bourikas, K.; Kordulis, C.; Lycourghiotis, A. The Role of the Liquid-Solid Interface in the Preparation of Supported Catalysts. *Catal. Rev.-Sci. Eng.* **2006**, *48*, 363–444. [CrossRef]
23. Cavallaro, S.; Mondello, N.; Freni, S. Hydrogen produced from ethanol for internal reforming molten carbonate fuel cell. *J. Power Sources* **2001**, *102*, 198–204.

24. Basagiannis, A.C.; Verykios, X.E. Catalytic steam reforming of acetic acid for hydrogen production. *Int. J. Hydrogen Energy* **2007**, *32*, 3343–3355. [CrossRef]
25. Wang, R.; Li, Y.; Shi, R.; Yang, M. Effect of metal-support interaction on the catalytic performance of Ni/Al_2O_3 for selective hydrogenation of isoprene. *J. Mol. Catal. A* **2011**, *344*, 122–127. [CrossRef]
26. Machida, M.; Eguchi, K.; Arai, H. Effect of Additives on the Surface Area of Oxide Supports for Catalytic Combustion. *J. Catal.* **1987**, *103*, 385–393. [CrossRef]
27. Wang, Y.; Wang, L.; Gan, N.; Lim, Z.Y.; Wu, C.Z.; Peng, J.; Wang, W.G. Evaluation of $Ni/Y_2O_3/Al_2O_3$ catalysts for hydrogen production by autothermal reforming of methane. *Int. J. Hydrogen Energy* **2014**, *39*, 10971–10979. [CrossRef]
28. Boukha, Z.; Jiménez González, C.; de Rivas, B.; GonzálezVelasco, J.R.; Gutiérrez Ortiz, J.I.; López Fonseca, R. Synthesis, characterisation and performance evaluation of spinel-derived Ni/Al_2O_3 catalysts for various methane reforming reactions. *Appl. Catal. B* **2014**, *158–159*, 190–201. [CrossRef]
29. Yang, R.; Zhang, Z.; Wu, J.; Li, X.; Wang, L. Hydrotreating Performance of La-Modified Ni/Al_2O_3 Catalysts Prepared by Hydrothermal Impregnation Method. *Kinet. Catal.* **2015**, *56*, 222–225. [CrossRef]
30. Daza, C.E.; Gallego, J.; Mondragon, F.; Moreno, S.; Molina, R. High stability of Ce-promoted Ni/Mg-Al catalysts derived from hydrotalcites in dry reforming of methane. *Fuel* **2010**, *89*, 592–603. [CrossRef]
31. Debek, R.; Radlik, M.; Motak, M.; Galvez, M.E.; Turek, W.; da Costa, P.; Grzybek, T. Ni-containing Ce-promoted hydrotalcite derived materials as catalysts for methane reforming with carbon dioxide at low temperature—On the effect of basicity. *Catal. Today* **2015**, *257*, 59–65. [CrossRef]
32. Damyanova, S.; Pawelec, B.; Arishtirova, K.; Fierro, J.L.G. Ni-based catalysts for reforming of methane with CO_2. *Int. J. Hydrogen Energy* **2012**, *37*, 15966–15975. [CrossRef]
33. Kraleva, E.; Pohl, M.-M.; Jurgensen, A.; Ehrich, H. Hydrogen production by bioethanol partial oxidation over Ni based catalysts. *Appl. Catal. B* **2015**, *179*, 509–520. [CrossRef]
34. Zaungouei, M.; Moghaddam, A.Z.; Arasteh, M. The Influence of Nickel Loading on Reducibility of NiO/Al_2O_3 Catalysts Synthesized by Sol-Gel Method. *Chem. Eng. Res. Bull.* **2010**, *14*, 97–102.
35. Kaynar, A.D.D.; Dogu, D.; Nail, Y. Hydrogen production and coke minimization through reforming of kerosene over bi-metallic ceria-alumina supported Ru-Ni catalysts. *Fuel Process. Technol.* **2015**, *140*, 96–103. [CrossRef]
36. Christensen, K.O.; Chen, D.; Lodeng, R.; Holmen, A. Effect of supports and Ni crystal size on carbon formation and sintering during steam methane reforming. *Appl. Catal. A* **2006**, *314*, 9–22. [CrossRef]
37. Quitete, C.P.B.; Bittencourt, R.C.P.; Souza, M.M.V.M. Coking resistance evaluation of tar removal catalysts. *Catal. Commun.* **2015**, *71*, 79–83. [CrossRef]
38. Fajardo, H.V.; Longo, E.; Mezalira, D.Z.; Nuernberg, G.B.; Almerindo, G.I.; Collasiol, A.; Probst, L.F.D.; Garcia, I.T.S.; Carreño, N.L.V. Influence of support on catalytic behavior of nickel catalysts in the steam reforming of ethanol for hydrogen production. *Environ. Chem. Lett.* **2010**, *8*, 79–85. [CrossRef]
39. Zou, X.; Wang, X.; Li, L.; Shen, K.; Lu, X.; Ding, W. Development of highly effective supported nickel catalysts for pre-reforming of liquefied petroleum gas under low steam to carbon molar ratios. *Int. J. Hydrogen Energy* **2010**, *35*, 12191–12200. [CrossRef]
40. Shekhawat, D.; Gardner, T.H.; Berry, D.A.; Salazar, M.; Haynes, D.J.; Spivey, J.J. Catalytic partial oxidation of *n*-tetradecane in the presence of sulfur or polynuclear aromatics: Effects of support and metal. *Appl.Catal. A* **2006**, *311*, 8–16. [CrossRef]
41. Wagner, C.D.; Davis, L.E.; Zeller, M.V.; Taylor, J.A.; Raymond, R.H.; Gale, L.H. Empirical atomic sensitivity factors for quantitative analysis by electron spectroscopy for chemical analysis. *Surf. Interface Anal.* **1981**, *3*, 211–225. [CrossRef]
42. Wagner, C.D.; Riggs, W.M.; Davis, L.E.; Moulder, J.F.; Muilenberg, G.E. *Handbook of X-ray Photoelectron Spectroscopy*; Perkin-Elmer Corp: Eden Prairie, MN, USA, 1979.
43. Spanos, N.; Matralis, H.K.; Kordulis, C.; Lycourghiotis, A. Molybdenum-oxo Species Deposited on Titania by Adsorption and Characterization of the Calcined Samples. *J. Catal.* **1992**, *136*, 432–445. [CrossRef]